Total Forward and Differential Cross Sections of Neutral D Mesons Produced in 500 GeV/c π^-–Nucleon Interactions

Fermilab E791 Collaboration

E. M. Aitala [i], S. Amato [a], J. C. Anjos [a], J. A. Appel [e], D. Ashery [n], S. Banerjee [e], I. Bediaga [a], G. Blaylock [h], S. B. Bracker [o], P. R. Burchat [m], R. A. Burnstein [f], T. Carter [e], H. S. Carvalho [a], N. K. Copty [ℓ], L. M. Cremaldi [i], C. Darling [r], K. Denisenko [e], S. Devmal [c], A. Fernandez [k], G. F. Fox [ℓ], P. Gagnon [b], C. Gobel [a], K. Gounder [i], A. M. Halling [e], G. Herrera [d], G. Hurvits [n], C. James [e], P. A. Kasper [f], S. Kwan [e], D. C. Langs [ℓ], J. Leslie [b], B. Lundberg [e], J. Magnin [a], S. MayTal-Beck [n], B. Meadows [c], J. R. T. de Mello Neto [a], D. Mihalcea [g], R. H. Milburn [p], J. M. de Miranda [a], A. Napier [p], A. Nguyen [g], A. B. d'Oliveira [c,k], K. O'Shaughnessy [b], K. C. Peng [f], L. P. Perera [c], M. V. Purohit [ℓ], B. Quinn [i], S. Radeztsky [q], A. Rafatian [i], N. W. Reay [g], J. J. Reidy [i], A. C. dos Reis [a], H. A. Rubin [f], D. A. Sanders [i], A. K. S. Santha [c], A. F. S. Santoro [a], A. J. Schwartz [c], M. Sheaff [d,q], R. A. Sidwell [g], A. J. Slaughter [r], M. D. Sokoloff [c], J. Solano [a], N. R. Stanton [g], R. J. Stefanski [e], K. Stenson [q], D. J. Summers [i], S. Takach [r], K. Thorne [e], A. K. Tripathi [g], S. Watanabe [q], R. Weiss-Babai [n], J. Wiener [j], N. Witchey [g], E. Wolin [r], S. M. Yang [g], D. Yi [i], S. Yoshida [g], R. Zaliznyak [m], and C. Zhang [g]

[a] *Centro Brasileiro de Pesquisas Físicas, Rio de Janeiro, Brazil*

[b] *University of California, Santa Cruz, California 95064, USA*

[c] *University of Cincinnati, Cincinnati, Ohio 45221, USA*

[d] *CINVESTAV, 07000 Mexico City, DF Mexico*

[e] *Fermilab, Batavia, Illinois 60510, USA*

[f] *Illinois Institute of Technology, Chicago, Illinois 60616, USA*

[g] *Kansas State University, Manhattan, Kansas 66506, USA*

[h] University of Massachusetts, Amherst, Massachusetts 01003, USA
[i] University of Mississippi–Oxford, University, Mississippi 38677, USA
[j] Princeton University, Princeton, New Jersey 08544, USA
[k] Universidad Autonoma de Puebla, Mexico
[ℓ] University of South Carolina, Columbia, South Carolina 29208, USA
[m] Stanford University, Stanford, California 94305, USA
[n] Tel Aviv University, Tel Aviv 69978, Israel
[o] Box 1290, Enderby, British Columbia V0E 1V0, Canada
[p] Tufts University, Medford, Massachusetts 02155, USA
[q] University of Wisconsin, Madison, Wisconsin 53706, USA
[r] Yale University, New Haven, Connecticut 06511, USA

Abstract

We measure the neutral D total forward cross section and the differential cross sections as functions of Feynman-x (x_F) and transverse momentum squared for 500 GeV/c π^-–nucleon interactions. The results are obtained from 88 990±460 reconstructed neutral D mesons from Fermilab experiment E791 using the decay channels $D^0 \to K^-\pi^+$ and $D^0 \to K^-\pi^+\pi^-\pi^+$ (and charge conjugates). We extract fit parameters from the differential cross sections and provide the first direct measurement of the turnover point in the x_F distribution, 0.0131±0.0038. We measure an absolute $D^0 + \overline{D}^0$ ($x_F > 0$) cross section of 15.4 $^{+1.8}_{-2.3}$ μbarns/nucleon (assuming a linear A dependence). The differential and total forward cross sections are compared to theoretical predictions and to results of previous experiments.

Key words:
PACS: 13.87.Ce 14.40.Lb 13.60.Le 25.80.Hp

Charm hadroproduction is a convolution of short range processes that can be calculated in perturbative quantum chromodynamics (QCD) and long range processes that cannot be treated perturbatively and thus must be modeled using experimental measurements. The large theoretical uncertainties from both contributions are reflected in the relatively large number of input parameters that can be adjusted when comparing models to the results of experiments. A single measurement, no matter how precise, cannot unambiguously determine these parameters. However, the results of high statistics measurements like the ones reported here, when combined with other measurements of similar precision, can constrain such parameters as the charm quark mass, the intrinsic transverse momentum of the partons in the incoming hadrons, and the effective factorization and renormalization scales used in theoretical calculations.

We report here measurements of the differential cross sections versus the kinematic variables Feynman-x (x_F) and transverse momentum squared (p_T^2), as well as the total forward cross section for the hadroproduction of neutral D mesons. The relatively high pion beam momentum, 500 GeV/c, coupled with the good geometric acceptance of the Tagged Photon Laboratory (TPL) spectrometer, allows us to investigate a wide kinematic region that includes points at negative x_F. We are able to measure the shape of the differential cross section versus x_F with sufficient precision to confirm, for the first time, that the turnover in the cross section does occur at $x_F{>}0$, as expected for incident pions [1].

Combining data from two D^0 decay modes, $D^0 \to K\pi$ and $D^0 \to K\pi\pi\pi$, [1] we extract a sample of 88 990±460 (78730±430 at $x_F{>}0$) fully reconstructed charm decays to use for these measurements. In addition to the greater statistical significance, the use of two modes provides a means to better understand the systematic errors associated with the reconstruction of the decay products of these fully-charged decays.

The data were accumulated during the 1991/1992 Fermilab fixed-target run of experiment E791 [2,3]. The experiment utilized the spectrometer built by the previous TPL experiments, E516 [4], E691 [5], and E769 [6], with significant improvements. The experiment employed a 500 GeV/c π^- beam tracked by eight planes of proportional wire chambers (PWC's) and six planes of silicon microstrip detectors (SMD's). The beam impinged on one 0.52-mm thick platinum foil (1.6 cm in diameter) followed by four 1.56-mm thick diamond foils (1.4 cm in diameter), each foil center separated from the next by an average of 1.53 cm, allowing most charm particles to decay in air. The downstream spectrometer consisted of 17 planes of SMD's for vertexing and tracking along with 35 planes of drift chambers, 2 PWC planes, and 2 analysis magnets (bending in the same direction) for track and momentum measurement. Two multi-cell threshold Čerenkov counters, an electromagnetic calorimeter, a hadronic calorimeter, and a wall of scintillation counters for muon detection provided particle identification. The trigger was generated using signals from scintillation counters as well as the electromagnetic and hadronic calorimeters. The beam scintillation counters included a beam counter 1.3 cm in diameter (14 cm upstream of the first target) and a large beam-halo veto counter with a 1.0 cm hole (8 cm upstream of the first target). The interaction counter was located 2.0 cm downstream of the last target and 0.6 cm upstream of the first SMD plane. The first-level trigger required a signal corresponding to at least 1/2 of that expected for a minimum ionizing particle (MIP) in the beam counter, no signal greater than 1/2 of a MIP in the beam halo counter, and a signal corresponding to greater than ∼4.5 MIP's in the interaction counter (consistent

[1] Charge conjugates are always implied. We use D^0 to represent the sum of D^0 and $\overline{D}^0$. Similarly, $K\pi$ ($K\pi\pi\pi$) includes $K^-\pi^+$ ($K^-\pi^+\pi^-\pi^+$) and charge conjugate.

with a hadronic interaction in one of the targets). The second-level trigger required more than 3 GeV of transverse energy in the calorimeters. Additional requirements eliminated events with multiple beam particles. A fast data acquisition system [7] collected data at rates up to 30 Mbyte/s with 50 μs/event deadtime. Over 2×10^{10} events were written to 24 000 8mm magnetic tapes during a six-month period.

The raw data were reconstructed and filtered [3,8] to keep events with at least two separated vertices, consistent with a primary interaction and a charm particle decay. Following the event reconstruction and filtering, selection criteria for the D^0 candidates were determined by maximizing $S/\sqrt{S+B}$ where S is the (normalized) number of signal events resulting from a Monte Carlo simulation and B is the number of background events appearing in the data sidebands of the reconstructed $K\pi$ or $K\pi\pi\pi$ mass distribution. Only selection variables that are well modeled by the Monte Carlo simulation were used. The final selection criteria varied by decay type ($K\pi$ and $K\pi\pi\pi$) and by x_F region. The full range of a cut variation is given in the descriptions below. To eliminate generic hadronic interaction backgrounds as well as secondary interactions, the secondary vertex was required to be longitudinally separated from the primary vertex by more than 8-11 times the measurement uncertainty on the longitudinal separation ($\sim$400 μm) and to lie outside of the target foils. Backgrounds from the primary interaction were also reduced by requiring that the candidate decay tracks miss the primary vertex by at least 20-40 μm. To ensure a correctly reconstructed charm particle and primary vertex, the momentum vector of the D^0 candidate was required to point back to within 35-60 μm of the primary vertex and to have a momentum component perpendicular to the line connecting the primary and secondary vertices of less than 350-450 MeV/c. Finally, the sum of the squares of the transverse momenta of the decay tracks relative to the candidate D^0 momentum vector was required to be greater than 0.4 (GeV/c)^2 (0.15 (GeV/c)^2) for the $K\pi$ ($K\pi\pi\pi$) candidates to favor the decay of a high-mass particle. All primary vertices were required to occur in the diamond targets. Thus, our results come from a light, isoscalar target. The Čerenkov information is not used in this analysis; all particle-identification combinations are tried. The inclusive $K\pi$ and $K\pi\pi\pi$ signals are shown in Fig. 1.

The reconstructed data were split into 20 bins of x_F, integrating over all p_T^2, and 20 bins of p_T^2, integrating over $x_F>0$. To combine data from varied conditions (e.g., using particles that pass through one and two magnets), the normalized mass (m_n) is constructed for each candidate using its calculated mass and error (m and σ_m) and the measured mean mass (m_D): $m_n \equiv \frac{m-m_D}{\sigma_m}$. Using the binned maximum likelihood method, the normalized mass distributions were fit to a simple Gaussian for the signal and linear or quadratic polynomials for the background.

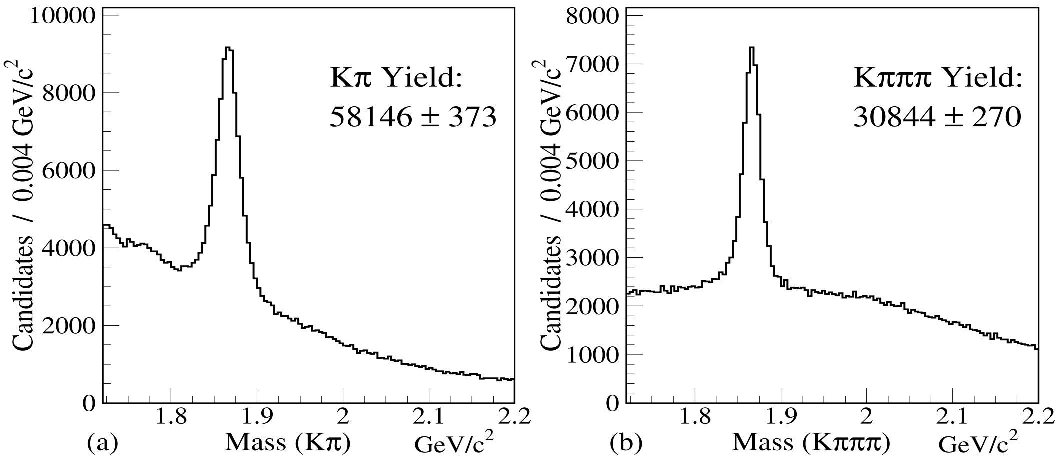

Fig. 1. The $K\pi$ and $K\pi\pi\pi$ signals for data with $-0.125<x_F<0.8$.

The acceptance can be factorized into trigger efficiency (ϵ_{trig}) and reconstruction efficiency (ϵ_{rec}). Most of the trigger inefficiency is due to vetoes on multiple beam particles. These resulted in a (70.3±1.1±4.2)% trigger efficiency, where the first error is statistical and the second error is systematic. The interaction and transverse energy requirements were greater than 99% efficient for reconstructable hadronic charm decays. Writing and reading the data tapes was (97.6±1.0)% efficient. Combining these efficiencies gives $\epsilon_{trig} = (68.3 \pm 4.4)\%$, where the error is dominated by the systematic error. The reconstruction efficiency is obtained from a Monte Carlo simulation. The Monte Carlo simulation used PYTHIA/JETSET [9] as a physics generator and models the effects of resolution, geometry, magnetic fields, and detector efficiencies as well as all analysis cuts. The efficiencies were separately modeled for five evenly spaced temporal periods during the experiment. This was motivated by a highly inefficient region of slowly increasing size in the center of the drift chambers caused by the 2 MHz pion beam. The Monte Carlo events were weighted to match the observed data distributions of x_F, p_T^2, and the summed p_T^2 of all two-magnet charged tracks in the event other than those from the candidate D meson. The resulting reconstruction efficiencies as a function of x_F and p_T^2 are shown in Fig. 2.

From the number of reconstructed D^0 candidates, the reconstruction efficiency, the trigger efficiency, and the PDG branching fractions [10], we obtain the number of D^0 mesons produced in our experiment during the experiment livetime, N_{prod}. The cross section as a function of each variable z (where $z = x_F$ or p_T^2), is:

$$\sigma(\pi^- N \rightarrow D^0 X; z) \quad = \quad \frac{N_{prod}(D^0; z)}{T_N \, N_{\pi^-}}. \tag{1}$$

T_N is the number of nucleons per area in the target (calculated from the target thickness) and is $(1.224 \pm 0.004) \times 10^{-6}$ nucleons/μb. N_{π^-} is the number of

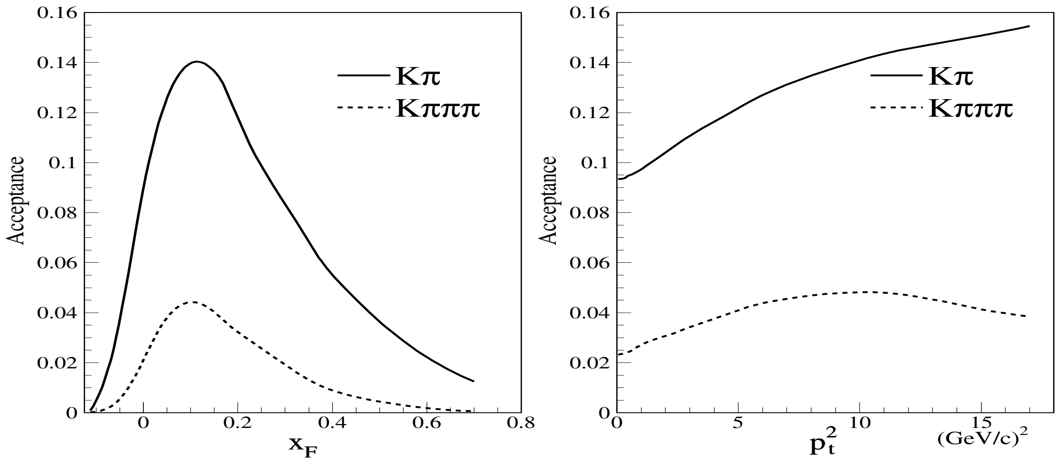

Fig. 2. $D^0 \to K\pi$ and $D^0 \to K\pi\pi\pi$ reconstruction efficiencies versus x_F (left) and p_T^2 (right).

incident π^- particles during the experiment livetime. This is obtained directly from a scaler which counted clean beam particles (>1/2 MIP signals in the beam and interaction counters and no signal greater than 1/2 MIP in the beam-halo veto counter) during the experiment livetime. These are the only beam particles which could cause a first-level trigger. Using Eq. 1, we obtained the $D^0+\overline{D}^0$ differential cross sections versus x_F and p_T^2 shown in Figs. 3 and 4.

The systematic errors are divided into two categories and incorporated in two stages. The *uncorrelated* systematic errors are determined individually for the $K\pi$ and $K\pi\pi\pi$ results. These systematic errors include uncertainties in the Monte Carlo modeling of the selection criteria, the background functions, and the widths used in the Gaussian signal functions. The *correlated* systematic errors are calculated for the combined D^0 result, obtained from adding the $K\pi$ and $K\pi\pi\pi$ samples together, weighted by the inverse-square of the combined statistical and uncorrelated systematic errors. The correlated errors are associated with uncertainties in the D^0 lifetime, the Monte Carlo production model, the Monte Carlo weighting procedure, and the run period weighting procedure. Finally, we compare our measured $K\pi$ to $K\pi\pi\pi$ branching ratio to the PDG [10] value to estimate the residual tracking and vertexing efficiency modeling error. In addition to these errors, which can affect both the normalization and the shape of the differential cross sections, there are two errors which affect only the normalization: the uncertainties in the trigger efficiency and target thickness.

For the differential cross sections shown in Figs. 3 and 4, the systematic errors are factorized into shape and normalization parts. The error bars in the figures show the sum, in quadrature, of the statistical and all systematic errors after factoring out the normalization component. Although the relative importance varies bin-by-bin, the most important systematic errors generally come from

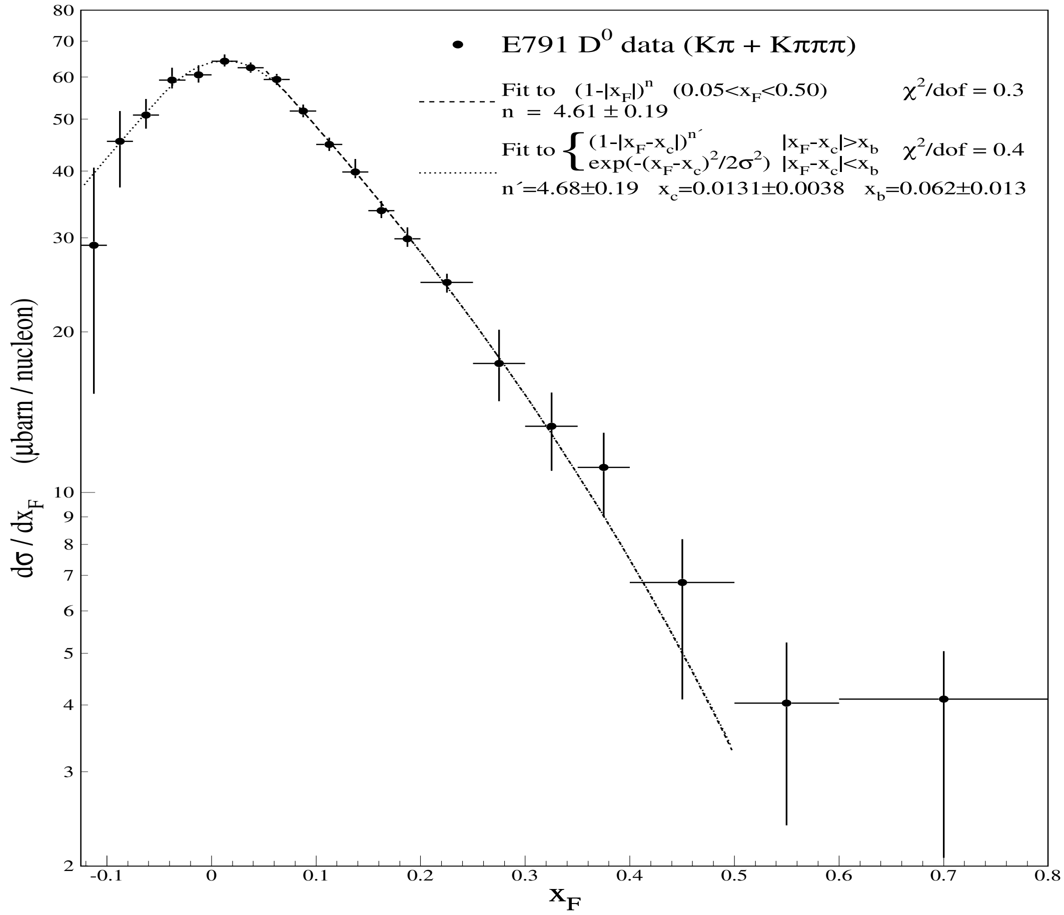

Fig. 3. Fits to the $D^0+\overline{D}^0$ x_F differential cross section with the functions given in Eqs. 2 (dashed) and 3 (dotted). Error bars do not include a $^{+10}_{-11}\%$ normalization uncertainty.

uncertainties in the signal width and the Monte Carlo efficiency modeling. In all cases, the systematic error dominates. For the total forward cross section, all of the errors are summarized and summed in Table 1.

In the past, x_F distributions have been fit with

$$\frac{d\sigma}{dx_F} = A(1-|x_F|)^n. \tag{2}$$

Fitting Eq. 2 in the range $0.05 < x_F < 0.50$, we find $n = 4.61 \pm 0.19$, as shown in Fig. 3. This function does not provide a complete representation of our data. Although the χ^2/dof is small (0.3), the value of n is quite dependent on the range fitted and on the errors on the data points. Another function, which can be extended into the negative x_F region, is an extension of Eq. 2 which uses a power-law function in the tail region and a Gaussian in the central region;

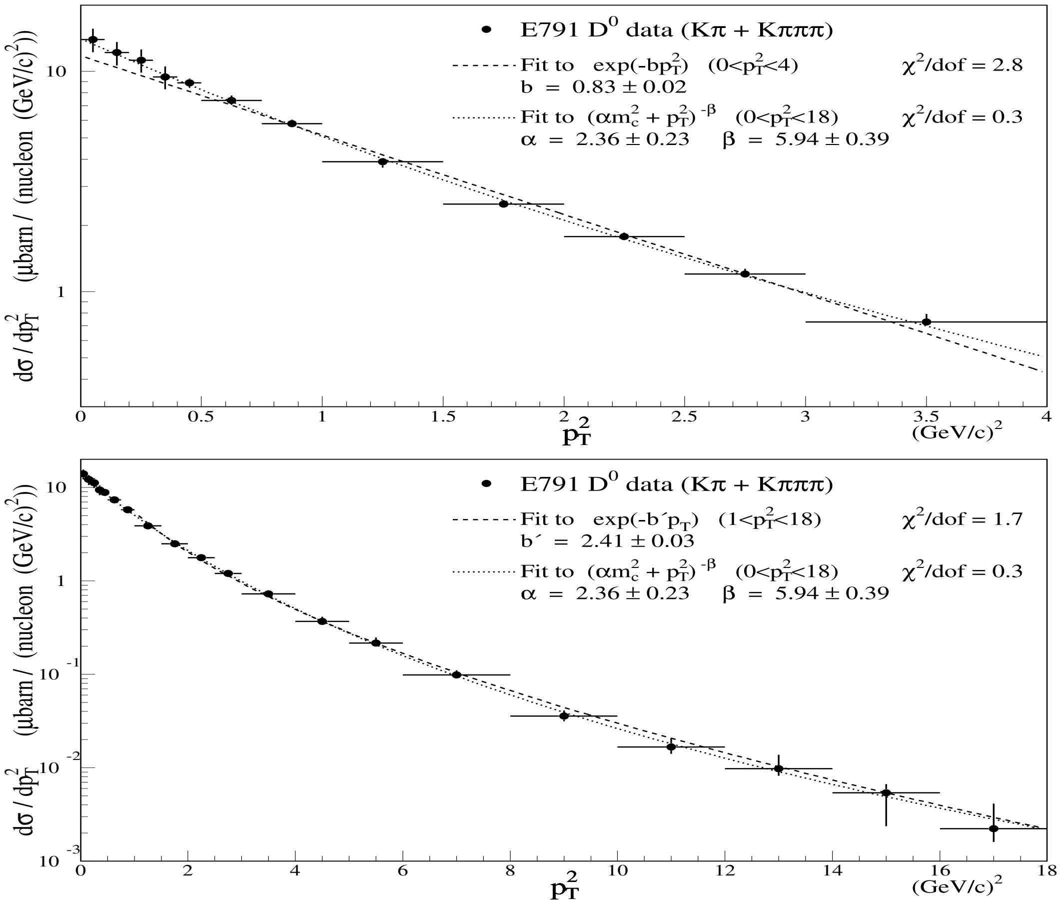

Fig. 4. Fits to the $D^0+\overline{D}^0$ p_T^2 differential cross section with the functions given in Eqs. 4 (dashed, top), 5 (dashed, bottom), and 6 (dotted, top and bottom). The top plot shows the range $0<p_T^2<4$ $(\mathrm{GeV}/c)^2$ while the bottom plot shows the full range, $0<p_T^2<18$ $(\mathrm{GeV}/c)^2$. Error bars do not include a $^{+11}_{-15}\%$ normalization uncertainty.

that is,

$$\frac{d\sigma}{dx_F} = \begin{cases} A(1-|x_F-x_c|)^{n'}, & |x_F-x_c|>x_b \\ A'\exp\left[-\frac{1}{2}(\frac{x_F-x_c}{\sigma})^2\right], & |x_F-x_c|<x_b \end{cases}. \tag{3}$$

Requiring continuous functions and derivatives allows us to write Eq. 3 with one normalization parameter and three shape parameters: n' gives the shape in the tail region, x_c is the turnover point, and x_b is the boundary between the Gaussian and power-law function. The fit parameters from this function are nearly independent of the fit range. Fitting our data in the range $-0.125<x_F<0.50$ gives $n' = 4.68 \pm 0.21$, $x_c = 0.0131 \pm 0.0038$, and $x_b = 0.062 \pm 0.013$ with a χ^2/dof=0.4, as shown in Fig. 3. This is the first measurement of the turnover point x_c in the charm sector. The fact that it is significantly greater than zero is consistent with a harder gluon distribution in the beam pions than in the target nucleons.

Table 1
Sources and values of the uncertainties on the total forward $D^0+\overline{D}^0$ cross section measurement. The total systematic error comes from the quadratic sum of the D^0 systematic errors. Although some of the systematic errors are subdivided, each D^0 systematic error is obtained directly (including correlations) and is not the quadratic sum of the components.

Error type	Error (%)		
	$K\pi$	$K\pi\pi\pi$	D^0
Statistical & uncorrelated systematic errors	$^{+4.7}_{-9.0}$	$^{+7.3}_{-11.0}$	$^{+4.7}_{-7.6}$
Statistics	±1.0	±2.8	
Selection criteria efficiency modeling	$^{+0.1}_{-0.0}$	$^{+1.2}_{-0.0}$	
MC background function	$^{+0.0}_{-5.5}$	$^{+0.0}_{-6.0}$	
D^0 signal width in fits	$^{+4.0}_{-4.1}$	$^{+3.9}_{-4.4}$	
PDG [10] branching ratio	±2.3	±5.3	
Correlated systematic errors			$^{+6.9}_{-9.9}$
D^0 lifetime	$^{+0.6}_{-0.5}$		
Monte Carlo kinematic weighting	$^{+0.0}_{-2.3}$		
Monte Carlo production model	$^{+5.9}_{-5.1}$		
Time dependent efficiency modeling	$^{+1.0}_{-2.0}$		
Tracking and vertex finding			±4.6
Trigger efficiency			±6.4
Target thickness			±0.3
Total			$^{+11.5}_{-14.8}$

The functions which have been used in the past to fit the p_T^2 distribution are:

$$\frac{d\sigma}{dp_T^2} = Ae^{-bp_T^2} \tag{4}$$

at low p_T^2 ($p_T^2 < 4.0$ (GeV/c)^2 for this analysis),

$$\frac{d\sigma}{dp_T^2} = Ae^{-b' p_T} \tag{5}$$

at high p_T^2 ($p_T^2 > 1.0$ (GeV/c)^2 for this analysis), and

$$\frac{d\sigma}{dp_T^2} = \left[\frac{A}{\alpha\, m_c^2 \,+\, p_T^2}\right]^\beta \tag{6}$$

over all p_T^2 with m_c set to 1.5 GeV/c^2 [11]. The results of fitting these equations to the data are shown in Fig. 4. For the ranges given above, the fit results are:

- $b = 0.83{\pm}0.02$ with $\chi^2/dof = 2.8$,
- $b' = 2.41{\pm}0.03$ with $\chi^2/dof = 1.7$, and
- $\alpha = 2.36{\pm}0.23$ $(\mathrm{GeV}/c^2)^{-2}$ and $\beta = 5.94{\pm}0.39$ with $\chi^2/dof = 0.3$.

Equation 4 does not provide a good fit even over the very limited range to which it is applied. While the χ^2/dof (1.7) of the fit to Eq. 5 is not good, it appears to be a reasonable fit to the data. Equation 6 provides a very good fit to the data over the entire range of p_T^2. Unfortunately, using two free parameters (in addition to the normalization) makes it more difficult to compare to other experiments and theory since the parameters in this fit are highly correlated. This is reflected in the large (7-10%) errors on α and β compared to the error on b' (1%), as shown above.

Figures 5 and 6 show a comparison of our x_F and p_T^2 distributions to theoretical predictions for charm quark and D meson production. Although the data come from D^0 mesons, the theoretical predictions for charm quark production are included for completeness. The theoretical curves are normalized to obtain the best fit (lowest χ^2/dof) to our data. The theoretical predictions come from a next-to-leading order (NLO) calculation by Mangano, Nason, and Ridolfi (MNR) [12] and the Pythia/Jetset [9] event generator. The MNR NLO charm quark calculation uses SMRS2 [13] (HMRSB [14]) NLO parton distribution functions for the pion (nucleon), a charm quark mass of 1.5 GeV/c^2, and an average intrinsic transverse momentum of the incoming partons ($\sqrt{\langle k_t^2 \rangle}$) of 1.0 GeV/$c$. The value for $\sqrt{\langle k_t^2 \rangle}$ was suggested by M. L. Mangano [15] and is independently motivated by the study of azimuthal angle correlations between two charm particles in the same event [11]. The D meson results are obtained by convoluting the charm quark results with the Peterson fragmentation function [16] with $\epsilon = 0.01$. The low value for ϵ was also suggested by M. L. Mangano [15] in response to a reanalysis of D fragmentation in e^+e^- collisions [17]. The Pythia/Jetset event generator uses leading order DO2 [18] (CTEQ2L [19]) parton distribution functions for the pion (nucleon), a charm quark mass of 1.35 GeV/c^2, $\sqrt{\langle k_t^2 \rangle}$ of 0.44 GeV/c, and the Lund string fragmentation scheme to obtain D^0 results. Tables 2 and 3 show a comparison of our x_F and p_T^2 fit results to theoretical predictions and to recent high-statistics charm experiments which used pion beams. The evident energy dependence of the shape parameters in Tables 2 and 3 are consistent with theoretical predictions [11].

We obtain the total forward cross section by summing the x_F differential cross section for $x_F{>}0$ and assuming the cross section for $0.8{<}x_F{<}1.0$ is half that of the cross section for $0.6{<}x_F{<}0.8$ but with the same error. Assuming a linear dependence on the atomic number [22], we obtain the neutral D total forward cross section, $\sigma(D^0 + \overline{D}^0; x_F > 0) = 15.4\ ^{+1.8}_{-2.3}$ μbarns/nucleon. To obtain

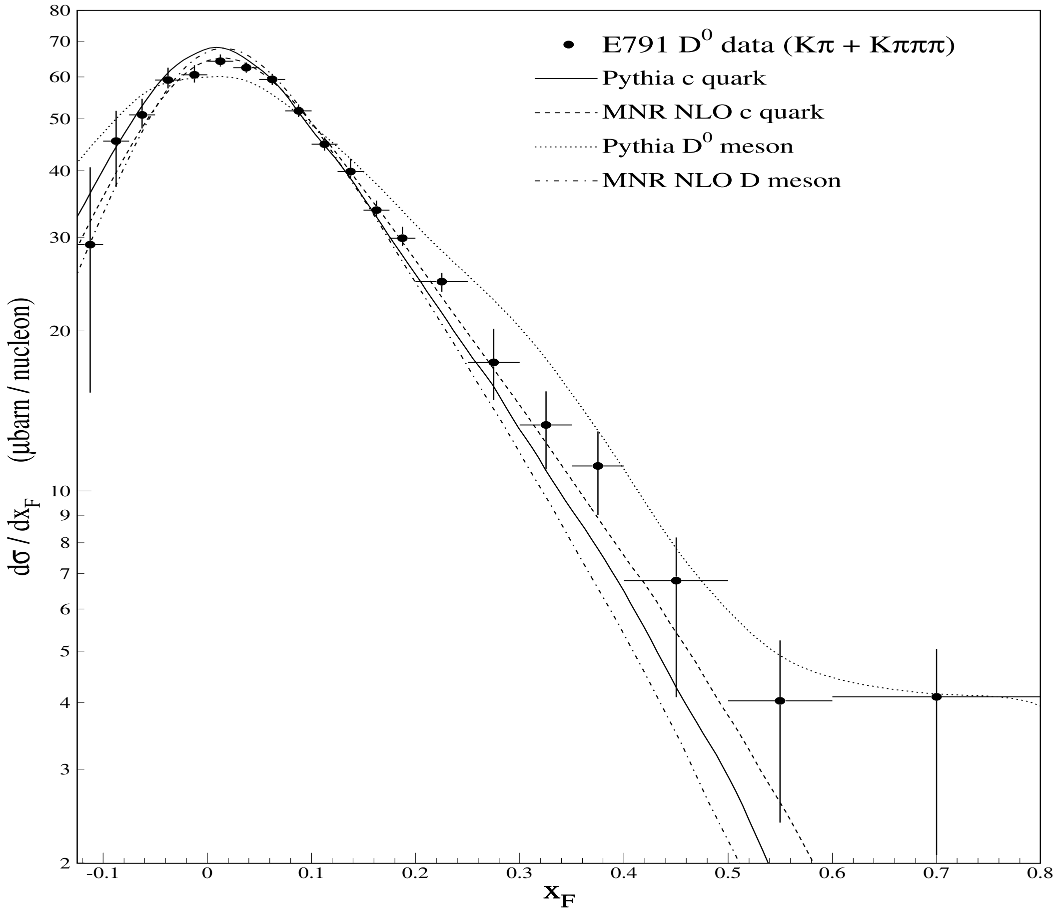

Fig. 5. The D^0+$\overline{D}^0$ x_F differential cross section compared to various theoretical predictions described in the text. The curves are normalized to obtain the best fit to the data in each case. Error bars do not include a $^{+10}_{-11}$% normalization uncertainty.

the total charm cross section, $\sigma(c\overline{c})$, we multiply our D^0+$\overline{D}^0$cross section by 1.7. This accounts for three multiplicative effects: the relative production of charm quarks compared to D^0 mesons (2.1), the conversion from x_F>0 to all x_F (1.6), and the conversion to the $c\overline{c}$ cross section from the sum of charm plus anticharm cross sections (0.5) [23]. We compare our total charm cross section to other experiments and to the NLO predictions as a function of pion-beam energy in Fig. 7. All experimental results are obtained by multiplying the D^0+$\overline{D}^0$cross section by 1.7. The rise of the charm production cross section with energy is modeled reasonably well by the NLO theory, although the absolute value at any point depends greatly on the input parameters to the theory.

In this paper we have presented the total forward cross section and differential cross sections versus x_F and p_T^2 for D^0 mesons from Fermilab experiment E791 data. This analysis represents the first measurement of the D^0 cross section for a 500 GeV/c pion beam. The high statistics allows us to clearly observe a turnover point greater than zero (x_c = 0.0131±0.0038) in the Feynman-x

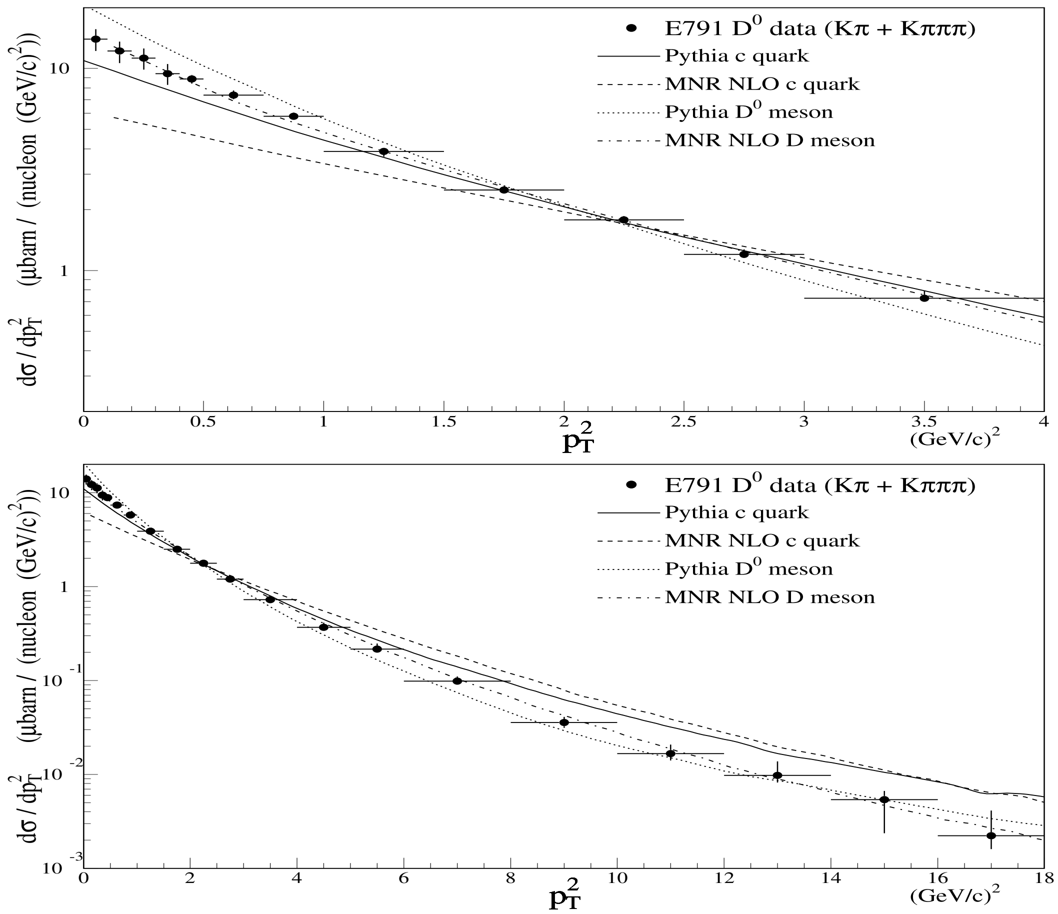

Fig. 6. The $D^0+\overline{D}^0$ p_T^2 differential cross section compared to various theoretical predictions described in the text. The curves are normalized to obtain the best fit to the data in each case. The top plot shows the range $0<p_T^2<4$ (GeV/c)^2 while the bottom plot shows the full range, $0<p_T^2<18$ (GeV/c)^2. Error bars do not include a $^{+11}_{-15}$% normalization uncertainty.

distribution, providing evidence for a harder gluon distribution in the pion than in the nucleon.

We have compared our differential cross section results to predictions from the next-to-leading order calculation by Mangano, Nason, and Ridolfi [12] and to the Monte Carlo event generator Pythia by T. Sjöstrand et al. [9]. With suitable choices for the intrinsic k_t of the partons and the Peterson fragmentation function parameter, the NLO D meson calculation provides a good match to the p_T^2 spectra and a fair match to the x_F distribution. The string fragmentation scheme in Pythia softens the original charm quark p_T^2 distribution too much, and hardens the x_F spectra too much in both directions. However, the D^0 result does predict the flattening of the x_F cross section at high x_F. The many adjustable parameters in the theoretical models allow one to obtain distributions which are quite consistent with these data. Unfortunately, a given set of parameters is neither unique, nor does it necessarily provide a good

Table 2
Comparison of x_F shape parameters to recent high-statistics pion-beam charm production experiments and to theory. E791 results are for D^0 mesons; E769 (WA92) results are from a combined sample of D^0, D^+, and D_s (D^0 and D^+) mesons. The theoretical results are obtained using the default parameters (described in the text). The fit range for n (Eq. 2) is in the table. The fit range for n' and x_c (Eq. 3) is $-0.125<x_F<0.50$.

Experiment	Energy (GeV)	x_F Range	n	n'	x_c
E791	500	0.05–0.5	4.61±0.19	4.68±0.21	.0131±.0038
WA92[20]	350	0.0–0.8	4.27±0.11		
E769[21]	250	0.0–0.8	4.03±0.18		
MNR NLO c	500	0.05–0.5	4.68	5.06	0.0231
MNR NLO D	500	0.05–0.5	5.53	6.00	0.0237
Pythia c	500	0.05–0.5	5.01	5.12	0.0115
Pythia D^0	500	0.05–0.5	3.62	3.66	0.0041

Table 3
Comparison of p_T^2 shape parameters to recent high-statistics pion-beam charm production experiments and to theory. Data samples are as described in Table 2. The fit range for b (Eq. 4) is $0<p_T^2<4$ (GeV/c)^2 except for WA92 which is $0<p_T^2<7$ (GeV/c)^2. The functions used to extract b' (Eq. 5) and α, β (Eq. 6) are fit in the range $p_T^2>1$ (GeV/c)^2 and $p_T^2<18$ (GeV/c)^2, respectively.

Experiment	Energy (GeV)	b (GeV/c)^2	b' (GeV/c)$^{-2}$	α (GeV/c)$^{-1}$	β
E791	500	0.83±0.02	2.41±0.03	2.36±0.23	5.94±0.39
WA92[20]	350	0.89±0.02			
E769[21]	250	1.08±0.05	2.74±0.09	1.4±0.3	5.0±0.6
MNR NLO c	500	0.57	1.88	6.20	8.68
MNR NLO D	500	0.94	2.32	1.99	5.30
Pythia c	500	0.77	2.09	2.32	5.14
Pythia D^0	500	1.06	2.58	1.55	5.07

match to other data. In conjunction with other charm production results from this and other recent high-statistics experiments, however, it may be possible to find a unique set of parameters. These results come from experiments with a variety of beam energies and types, and include measurements of differential cross sections [20,28,31], production asymmetries [20,28–31,33], and

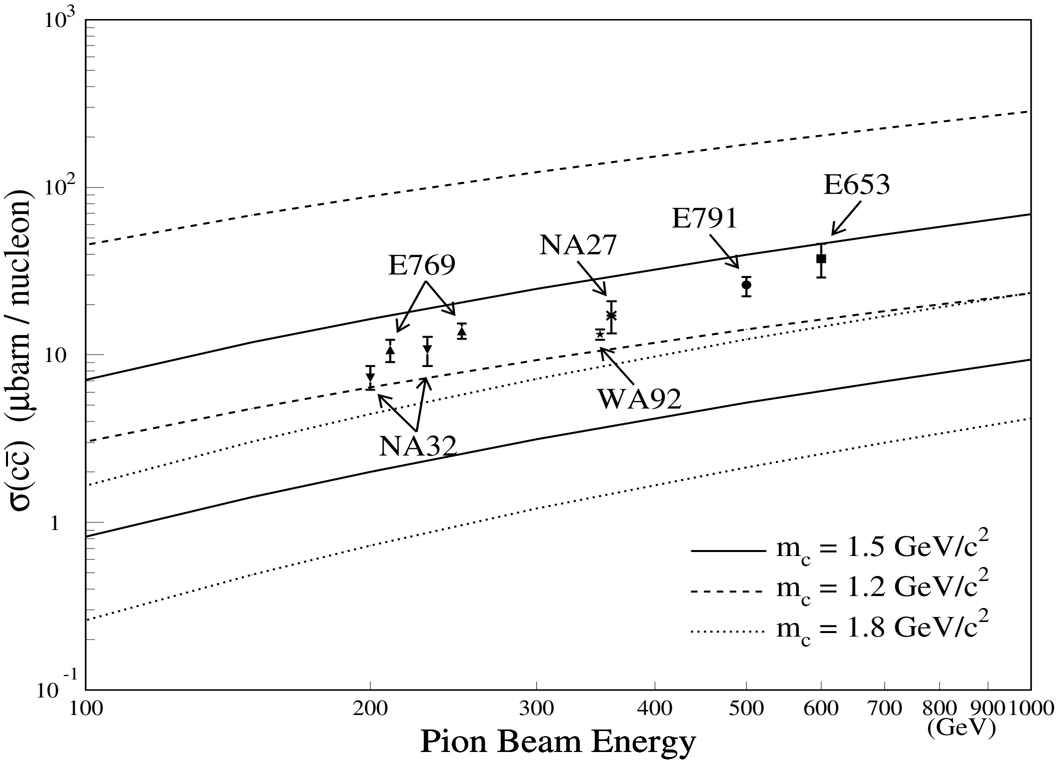

Fig. 7. Theoretical and experimental results for the π–N $\to c\bar{c}$ cross section versus energy. The theoretical curves are obtained from MNR NLO predictions [23]. The three bands (solid, dashed, and dotted) correspond to three different charm quark masses (1.5, 1.2, and 1.8 GeV/c^2). The variation within the bands comes only from varying the renormalization scale. The factorization scale is kept fixed. All experimental data points are 1.7 times the single inclusive D^0+$\overline{D}^0$ x_F>0 cross sections. The E653, NA27, WA92, NA32 (200 GeV), NA32 (230 GeV), and E769 data were obtained from references [24], [25], [20], [26], [27], and [28], respectively.

correlations between two charm particles in the same event [3,35,36].

Unlike the uncertainties in the theoretical calculations of the differential cross sections, the uncertainties in the theoretical calculation of the total cross section come mostly from the perturbative calculation. The relatively large uncertainties are due to the low mass of the charm quark, which results in a large (unknown) contribution from higher-order terms. The total forward D^0+$\overline{D}^0$ cross section measured by E791 is $\sigma(D^0 + \overline{D}^0\ ; x_F > 0)\ =\ 15.4\ ^{+1.8}_{-2.3}$ μbarns/nucleon, assuming a linear atomic number dependence. The cross section is consistent with the MNR NLO prediction.

We express our special thanks to S. Frixione, M. L. Mangano, P. Nason, and G. Ridolfi for the use, and help in the use, of their NLO QCD software. We gratefully acknowledge the assistance from Fermilab and other participating institutions. This work was supported by the Brazilian Conselho Nacional de Desenvolvimento Científico e Technológico, CONACyT (Mexico), the Israeli Academy of Sciences and Humanities, the U.S. Department of Energy, the U.S.-Israel Binational Science Foundation, and the U.S. National Science Foundation.

References

[1] R. K. Ellis and C. Quigg, FERMILAB-FN-445 (January 1987).

[2] J. A. Appel, Ann. Rev. Nucl. Part. Sci. **42** (1992) 367; D. J. Summers et al., Proceedings of the *XXVIIth Rencontre de Moriond*, Electroweak Interactions and Unified Theories, Les Arcs, France (15-22 March, 1992) 417.

[3] E791 Collaboration, E. M. Aitala et al., submitted to Eur. Phys. J. C, Fermilab-Pub-98-297-E, hep-ex/9809029 (September 1998).

[4] E516 Collaboration, K. Sliwa et al., Phys. Rev. D 32 (1985) 1053.

[5] E691 Collaboration, J. R. Raab et al., Phys. Rev. D 37 (1988) 2391.

[6] E769 Collaboration, G. A. Alves et al., Phys. Rev. Lett. 69 (1992) 3147.

[7] S. Amato et al., Nucl. Inst. and Meth. A324 (1992) 535.

[8] S. Bracker et al., IEEE Trans. Nucl. Sci. 43 (1996) 2457; F. Rinaldo and S. Wolbers, Comput. Phys. 7 (1993) 184.

[9] H.-U. Bengtsson and T. Sjöstrand, Comp. Phys. Comm. 82 (1994) 74; T. Sjöstrand, PYTHIA 5.7 and JETSET 7.4 Physics and Manual, CERN-TH.7112/93, 1995.

[10] Particle Data Group, Eur. Phys. J. C 3 (1998) 497.

[11] S. Frixione, M. L. Mangano, P. Nason, and G. Ridolfi, Nucl. Phys. B431 (1994) 453.

[12] M. L. Mangano, P. Nason, and G. Ridolfi, Nucl. Phys. B373 (1992) 295.

[13] P. J. Sutton et al., Phys. Rev. D 45 (1992) 2349.

[14] P. N. Harriman et al., Phys. Rev. D 42 (1990) 798.

[15] M. L. Mangano, hep-ph/9711337 (1997); M. L. Mangano, private communication (April 1999).

[16] C. Peterson et al., Phys. Rev. D 27 (1983) 105.

[17] M. Cacciari and M. Greco, Phys. Rev. D 55 (1997) 7134.

[18] D. W. Duke and J. F. Owens, Phys. Rev. D 30 (1984) 49.

[19] J. Botts et al., Phys. Lett. B304 (1993) 159.

[20] BEATRICE Collaboration, M. Adamovich et al., Nucl. Phys. B495 (1997) 3.

[21] E769 Collaboration, G. A. Alves et al., Phys. Rev. Lett. 77 (1996) 2392.

[22] E769 Collaboration, G. A. Alves et al., Phys. Rev. Lett. 70 (1993) 722.

[23] S. Frixione, M. L. Mangano, P. Nason, and G. Ridolfi, Heavy Flavours II, Advanced Series on Directions in High Energy Physics, 1997, hep-ph/9702287.

[24] E653 Collaboration, K. Kodama et al., Phys. Lett. B284 (1992) 461.

[25] LEBC-EHS Collaboration, M. Aguilar-Benitez et al., Phys. Lett. B161 (1985) 400.

[26] ACCMOR Collaboration, S. Barlag et al., Zeit. Phys. C 39 (1988) 451.

[27] ACCMOR Collaboration, S. Barlag et al., Zeit. Phys. C 49 (1991) 555.

[28] E769 Collaboration, G. A. Alves et al., Phys. Rev. Lett. 77 (1996) 2388.

[29] E791 Collaboration, E. M. Aitala et al., Phys. Lett. B371 (1996) 157; Phys. Lett. B411 (1997) 230.

[30] E769 Collaboration, G. A. Alves et al., Phys. Rev. Lett. 72 (1994) 812.

[31] SELEX Collaboration, F G. Garcia, S. Y. Jun, et al., to be published in the proceedings of American Physical Society (APS) Meeting of the Division of Particles and Fields (DPF 99), Los Angeles, CA, 5-9 Jan 1999, hep-ex/9905003.

[32] WA89 Collaboration, M. I. Adamovich et al., submitted to Eur. Phys. J. C, CERN-EP/98-41, hep-ex/9803021 (March, 1998).

[33] E687 Collaboration, P. L. Frabetti et al., Phys. Lett. B370 (1996) 222.

[34] WA82 Collaboration, M. Adamovich et al., Phys. Lett. B305 (1995) 402.

[35] BEATRICE Collaboration, M. Adamovich et al., Phys. Lett. B348 (1995) 256; Nucl. Phys. B495 (1997) 3; Phys. Lett. B385 (1996) 487.

[36] E687 Collaboration, P. L. Frabetti et al., Phys. Lett. B308 (1993) 193.